Electrochimica Acta 458 (2023) 142514

Contents lists available at ScienceDirect

Electrochimica Acta

journal homepage: www.journals.elsevier.com/electrochimica-acta

A spectroelectrochemical study of copper chloro-complexes for high performance all-copper redox flow batteries

Giampaolo Lacarbonara [1], Nicolò Albanelli [1], Daniele Fazzi, Catia Arbizzani [*,1]

Department of Chemistry "Giacomo Ciamician", Alma Mater Studiorum - University of Bologna, Via Francesco Selmi 2, Bologna 40126, Italy

ARTICLE INFO

Keywords:
Chlorocomplexes
Copper
Cluster solvation
Redox flow batteries
Spectroelectrochemistry

ABSTRACT

Redox Flow Batteries (RFB) are an ideal choice for large stationary applications. Among the different chemistries that can be exploited, all-copper aqueous RFB (CuRFB) use low-cost, earth-abundant raw materials with a well-defined European supply chain. The CuRFB takes advantage of the three oxidation states of copper. As Cu(I) is not stable in aqueous media, the system is based on the chlorocomplexation of the copper cations. We demonstrated that it is possible to evaluate the complexation characteristic of the concentrated solutions used in CuRFB by investigating the speciation of copper (II) in electrolytes with increasing Cu(II) concentration. Spectro-electrochemical tests in diluted solution give information on the electrochemical behavior of electrolytes with a different chloro-complexes distribution. Quantum chemical calculations elucidate the molecular structure and electronic transitions of water solvated copper chloro-complexes, thus complementing the experimental picture.

1. Introduction

The transition from fossil fuels to renewable power sources is facilitated by the rapid innovation of enabling technologies like energy storage systems. In order to satisfy the different needs of an increasingly electricity-based society, it is mandatory to develop storage systems with diversified functions [1]. Redox flow batteries (RFB) are an ideal choice for large energy scale application and combination to renewable sources such as solar, wind or tidal systems. Due to the dependency of the stored energy from the volume and the concentration of the electrolytes, RFBs represent a promising energy storage solution exhibiting a modular design and scalability. In addition, the decoupling of energy storage and power generation is a big advantage in the design and optimization of a RFB [2].

Among the different chemistries adopted in RFB systems, the Cu-based battery system appeared in 1974 [3] with copper perchlorate salt in acetonitrile and continued with chlorocuprate ionic liquids [4]. The studies in aqueous electrolytes by Sanz et al. [5] represented the groundwork for developing aqueous all-copper RFBs. The system proposed exploited the three different oxidation states of copper, Cu(0), (I) and Cu(II). Similarly to acetonitrile stabilization of Cu(I) as introduced by Kratochvil et al. [3], Sanz et al. used chlorides as complexing agents to stabilize the Cu(I) in an aqueous solution [5]. In fact, the electronic structure of the coordinated transition metal ions highly depends by the local molecular coordination, the solvent agent and the ionic strength [6].

The aqueous all-copper RFB is based on the stabilization of Cu(I) ions by complexation. However, the distribution of chloro-complexes species also determines the thermodynamics and kinetics of the electrochemical reaction, thus playing a crucial role in developing a highly performing CuRFB system [7–10]. Both Cu(I) and Cu(II) showed several species in a chloride-rich aqueous solution. For Cu(II), there are at least five species (Cu^{2+}, $[CuCl]^{+}$, $[CuCl_2]^{0}$, $[CuCl_3]^{-}$, and $[CuCl_4]^{2-}$), and there are at least six complexes for Cu(I) (Cu^{+}, $[CuCl]^{0}$, $[CuCl_2]^{-}$, $[CuCl_3]^{2-}$, $[Cu_2Cl_4]^{2-}$, and $[Cu_3Cl_6]^{3-}$). The distribution of these complexes strongly depends on the concentration of copper and chloride ions with respect to the solvent [11–16].

The evaluation of stability constants and competitive thermodynamic equilibria between the various complexes required many efforts [17–21]. However, many investigations were conducted without considering the ionic strength and the copper-to-solvent ratio. Thus, the studies provided different results due to the changes in the molecular environment and the complexation at different Cl^{-} concentrations.

Currently, to optimize the physical-chemical properties of new electrolytes for CuRFB is mandatory to pursue a deeper study of the stability of copper chloro-complexes in real solutions. The Bard's group

* Corresponding author.
E-mail address: catia.arbizzani@unibo.it (C. Arbizzani).
[1] ISE Members

https://doi.org/10.1016/j.electacta.2023.142514
Received 17 January 2023; Received in revised form 20 March 2023; Accepted 1 May 2023
Available online 2 May 2023
0013-4686/© 2023 The Authors. Published by Elsevier Ltd. This is an open access article under the CC BY license (http://creativecommons.org/licenses/by/4.0/).

carried out several studies in dilute solutions of copper [22,23] with ultramicroelectrodes (UME) accounting for the ionic strength's influence with the highest concentration of 0.5 M [22]. This work indicated that the main species of Cu(II) complexes in high chloride concentration is $[CuCl_4]^{2-}$ and the main species of Cu(I) complexes are $[CuCl_2]^-$ and $[CuCl_3]^{2-}$. They also proposed a model to determine the stability constant of the complex at various temperatures [23]. The increase of the temperature or the Cl^- concentration can avoid the formation of insoluble Cu(I)Cl intermediates that deactivate the electrode surface. However, the speciation of copper complexes in solution has not yet found a univocal description. The different salts used in solutions as chloride sources increase the difficulties because of their different ionic dissociation. In addition, differences in the solution's ionic strength impact on ion activity. Our approach is to relate the behavior of diluted $CuCl_2$ solutions (5 and 50 mM) to those of highly concentrated (0.5 and 2 M) solutions in which a low amount of free Cl^- and water are available for the complexation of Cu^{2+}. Kinetics and thermodynamics of the electrode reaction strongly depend on the stability of the electroactive species in solution. In RFB, the stability of the redox species determines the cell performance, such as coulombic efficiency, voltage efficiency, and energy efficiency. It is crucial, indeed, to elucidate the speciation of Cu(II) in concentrated CuRFB electrolytes to achieve the best performance. Moreover, detecting and avoiding any possible reason of failures for the long-term application becomes fundamental, in general, for RFBs [24].

To our knowledge, it is the first time that a spectroelectrochemical study of solutions at different concentration of Cu(II) is carried out in order to compare the response of dilute solutions to that of the most concentrated one (2 M), being the latter of practical interest for RFBs. To achieve such a goal, it has been necessary to shift the analysis from the UV–Vis region, where the absorption of chloro complexes is high even at low Cu(II) concentration, to the NIR region, where the most concentrated solution can be analyzed for the low molar extinction coefficient that allows the absorbance measurements even in highly concentrated regimes. During the cyclic voltammetry, the solution absorbance at two different wavelengths has been recorded. The absorbance at 385 nm wavelength has been selected to follow the formation and disappearance of highly coordinated complexes ($[CuCl_3]^-$ and $[CuCl_4]^{2-}$) during the voltammetric experiment. The absorbance at 870 nm was chosen instead to probe the presence of the Cu(II) species in solution. Insights into the structure of copper-chloride complexes formed in solution, and the assignments of the main electronic transitions in the UV–Vis-NIR spectrum have been based on semiempirical and quantum-chemical calculations carried out on supramolecular water solvated copper-chloride clusters. The spectrophotometric signals display hysteresis which is linked to the copper chlorocomplexes stability. The information from NIR absorption spectra can be used to lay the groundwork for a state of charge (SoC) optical monitoring systems [25].

2. Experimental section

2.1. Chemicals

The electrolytes were prepared with hydrochloric acid (37%, Sigma-Aldrich, Merck KGaA, Darmstadt, Germany) as supporting electrolytes and copper (II) chloride dehydrates (99.99 +%, Sigma Aldrich) and copper (I) chloride (>99.995% trace metal basis, Sigma Aldrich). After complete dissolution, the electrolytes were deaerated in Ar for ten minutes and sealed.

2.2. Spectrophotometric and spectroelectrochemical experiments

The absorption spectra were acquired with a Perkin Elmer Lambda19 UV/Vis/NIR Spectrophotometer (PerkinElmer, UK) in quartz cuvettes with 10 mm optical path (OP). To avoid problems of linearity in the Lambert-Beer law, the increasing of Cu(II) concentration was compensated by using different quartz spacers to decrease the OP to 1000, 300, and 50 μm. The percentage absorbance has been calculated subtracting the minimum at the absorbance values and dividing it by the maximum value.

The spectroelectrochemical measurements were carried out with PAR273A potentiostat/galvanostat and Lambda 19 Spectrophotometer in a spectroelectrochemical cell (ALS, Japan) with three-electrode setup and 0.25 mm OP. Pt mesh was used as working electrode (WE, 0.691 cm^2), Pt wire as counter electrode (CE) and Ag/AgCl reference electrode (RE, ALS, Japan) as reference electrode. All the solutions were deaerated for 15 min in Ar and the cuvette was sealed for maintaining the Ar atmosphere during the experiments. The spectroelectrochemical tests were carried out at room temperature.

2.3. Electrochemical experiments

The electrochemical properties of the electrolytes were evaluated on Pt disk working electrode (0.126 cm^2) in three-electrode conventional cell with a graphite rod counter electrode,a saturated Ag/AgCl reference electrode in separated compartments. The active area of the Pt mesh used as working electrode in the spectroelectrochemical cell was evaluated by cyclic voltammetry at 40 °C of 5 mM ferrocene methanol (FM, 97%, Sigma Aldrich) and phosphate buffer solution 1x (PBS, Oxoid itd, tablets) in the conventional three-electrode cell with a graphite rod (6 mm diameter, Gamry) as counter electrode and a saturated calomel electrode (SCE, AMEL, 303/SCG/6 J) as reference electrode with a Voltalab PGZ301 (Radiometer Copenhagen, Denmark) potentiostat/galvanostat. The peak current of the cyclic voltammetry at 40 °C on Pt mesh was compared to that on Pt disk (0.126 cm^2). All electrochemical tests in conventional cell were carried out at room temperature if not differently indicated.

3. Calculations

Copper-chloride molecular clusters, explicitly solvated with water molecules, were initially generated with the code Packmol [26], by considering cubic boxes of lateral length ranging from 10 to 20 Å. The copper-chloride molecular clusters considered were *i*) $[CuCl]^+$, *ii*) $[CuCl_2]^0$ and *iii*) $[CuCl_3]^-$, as coordinated with water molecules giving the (stoichiometric) supramolecular clusters $[CuCl(H_2O)_5]^+$, $[CuCl_2(H_2O)_4]^0$, and $[CuCl_3(H_2O)_3]^-$. To further investigate solvent effects as induced by a variable number of water molecules, each copper-chloride cluster *i*)-*iii*) was solvated with a number of water molecules ranging from 1 up to 200 (see explanatory examples in Supplementary Information).

The geometry optimization of each structure was initially performed at the semiempirical level, namely adopting the density functional tight-binding scheme GFN*n*-xTB (Geometry Frequency Non-covalent interactions-eXtended Tight Binding, specifically GFN2-xTB [27–29] (v. 6.4.1). For the stoichiometric supramolecular clusters $[CuCl(H_2O)_5]^+$, $[CuCl_2(H_2O)_4]^0$, and $[CuCl_3(H_2O)_3]^-$ GFN2-xTB meta-dynamics were carried out with the algorithm CREST (v 2.11) for sampling the conformational space [30]. Most stable conformers were optimized at the GFN2-xTB level with very-tight geometry-convergence thresholds and further re-optimized at the DFT level.

For the DFT calculations (i.e., geometry optimizations) the range-separated ωB97X-D functional was considered. For hydrogen, oxygen and chloride atoms the Pople split-valence double-zeta basis set with polarization functions 6–31G* was used, while for copper the fully relativistic pseudopotential ECP10MDF [31] with the double-zeta basis set ECP10MDF_VDZ [32] was adopted.

Excited states (up to 300 states) were calculated both at the semiempirical time-dependent DFT level, namely the Tamm-Dancoff sTDA and the sTD-DFT approaches [33], and at the TD-DFT level. DFT-based semiempirical calculations were carried out by using the code xTB [27]. DFT and TDDFT calculations were carried out by using the code Gaussian16 [34].

Optimized geometries of the supramolecular clusters $[CuCl(H_2O)_5]^+$, $[CuCl_2(H_2O)_4]^0$, and $[CuCl_3(H_2O)_3]^-$ (i.e., the clusters considered for interpreting the experimental data, vide infra) are reported in Supplementary Information. All other cluster geometries modelled in this work are available under request to the corresponding author.

4. Results and discussion

4.1. Cu(II) speciation dependence from HCl concentration

In RFBs, the electrolyte concentration is one of the most critical parameters that determine the energy of the whole system. The stabilization of Cu(I) by the chlorides complexing agents makes possible the employment of Cu(I) in CuRFB application. Hence, Cu(I) stabilization in aqueous environment represents an essential milestone to achieve valuable performance in an electrochemical cell. For this purpose, the addition of hydrochloric acid increases the conductivity of the solutions, and the chloride ions stabilize the Cu(I)/Cu(II) redox couple.

The distribution of Cu(II) chloride complexes at different copper and chloride concentrations were obtained from deconvolution of the UV/Vis spectra. In this region, the ligand-to-metal charge transfer (LMCT) transition gives information about the coordination of the copper cation. This transition, from 220 to 390 nm, has a band structure influenced by the degree of complexation of the cation [35]. In the quantitative analysis of the LMCT band, 50 mM Cu(II) is the concentration limit (optical path of 50 μm) to have a linear relationship between the absorbance and the Cu(II) concentration. Instead, the band investigation is limited by commonly used detectors to a Cu(II) concentration of 0.1 M for qualitative observations.

For the complexation equilibrium (1) and the equilibrium constant (2), the chloride concentration is more impacting than the copper concentration in the distribution of the complexes (3).

$$Cu(H_2O)_6^{2+} + nCl^- \rightleftharpoons CuCl_n(H_2O)_{6-n}^{2-n} + nH_2O \quad (1)$$

$$\beta_n = \frac{[CuCl_n(H_2O)_{6-n}^{2-n}][H_2O]^n}{[Cu(H_2O)_6^{2+}][Cl^-]^n} \quad (2)$$

$$[CuCl_n(H_2O)_{6-n}^{2-n}] = \beta_n [Cu(H_2O)_6^{2+}][Cl^-]^n \quad (3)$$

With a fixed 50 mM concentration of copper chloride, the HCl concentration was varied from 1 to 6 M. For each copper complex, the absorption spectrum was deconvoluted using Gaussian functions with the parameters obtained by the spectrophotometric data reported by Brugger et al. [35]. In the absorption spectrum of Fig. 1c, the contribution at c.a. 280 nm (cyan curve) is given by the overlapping of the absorption band of both $[CuCl_2]^0$, $[CuCl_3]^-$ and $[CuCl_4]^{2-}$ complexes. The high superimposition of the three contributions in the 260–310 nm spectral region makes difficult the deconvolution of this part of the spectrum. After having identified a spectral region in which only one complex absorbs, the absorbance can be used to estimate the percentual composition of the chlorocomplexes (Fig. 2). For $[CuCl_2]^0$ and $[CuCl_3]^-$ + $[CuCl_4]^{2-}$ complexes, the distributions were obtained from the band at 210–260 and 340–420 nm, respectively. In the 1 M HCl solution (Fig. 1a), the mainly prevalent complex is the $[Cu(H_2O)_6]^{2+}$, with a gradually smaller presence of $[CuCl]^+$ and $[CuCl_2]^0$. Increasing the HCl concentration to 3 M (Fig. 1b), there is a red shift of the LMCT band from 250 nm to 258 nm, indicating a higher concentration of the $[CuCl_2]^0$ (absorbing at 277 nm). At a concentration of HCl of 6 M, a small band at 384 nm indicates the presence of highly coordinated complexes which display two bands at 273 nm and 384 nm. According to Eq. (2), highly coordinated copper complexes become favoured by increasing chloride concentration. However, the percentage distribution indicates that $[CuCl_4]^{2-}$ seems to be not present even at 6 M Cl^- concentration, although its presence in traces cannot be excluded. The results partially agree with the distributions presented in literature [21,22,35].

However, a clear definition for the speciation of copper complexes in solution is still needed. Indeed, different descriptions are not in agreement with each other. Due to their different ionic dissociation, the various salts used in solutions as chloride sources make the situation challenging. Ion activity is also affected by variations in the solution's ionic strength. In Bard's group works [22,23], $[CuCl_4]^{2-}$ species predominated at free chloride concentrations of 10 M [22], while by taking into account the mean ionic activity coefficient [23], the chlorocomplex distribution is quite different. Specifically, the fractional distribution proposed for 7 mol/L considering the mean ionic coefficient at 25 °C indicates that $[CuCl_2]$ and $[CuCl_4]^{2-}$ are mostly present, and $[CuCl_3]^-$ has a slightly lower percentage [23].

In our investigation, the fractional distribution was obtained from experimental UV–Vis spectra and perfectly agreed with the spectroscopic results reported by Brugger in Ref. [35]. The presence of $[CuCl_4]^{2-}$ should be negligible by considering only the results reported by Brugger's group. Although from the spectra it is not possible to separate the contributions of $[CuCl_3]^-$ and $[CuCl_4]^{2-}$ because they are very similar, the presence of $[CuCl_4]^{2-}$ could be confirmed by the fact that increasing the Cl^- concentration up to 9 M (Fig. S1) causes an

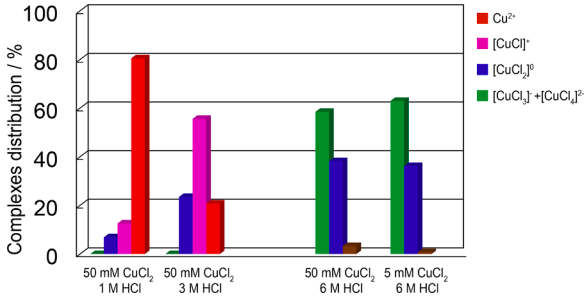

Fig. 2. Cu(II) chlorocomplexes distribution at different concentrations of HCl (1 M, 3 M and 6 M) and $CuCl_2$, as obtained by the deconvolution procedure of the UV/Vis spectra.

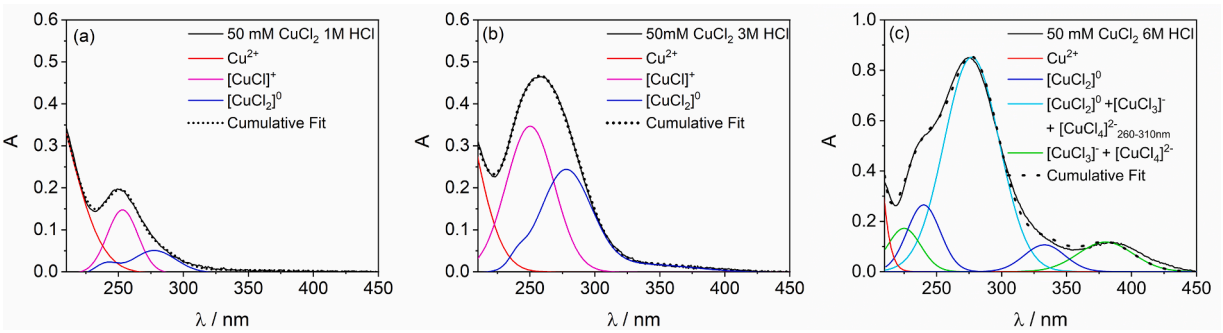

Fig. 1. UV/Vis absorption spectra of 50 mM $CuCl_2$ electrolytes with different concentrations of HCl ((a) 1 M, (b) 3 M, (c) 6 M) in quartz cuvette (OP 50 μm).

absorption decrease of the component at 240 nm that could be attributed to the increase of the $[CuCl_4]^{2-}$ species. Therefore, the 350–410 nm transition could be ascribed to the sum of $[CuCl_3]^-$ and $[CuCl_4]^{2-}$, indicating a fractional distribution of 40% $[CuCl_2]$ and 60% $[CuCl_3]^- + [CuCl_4]^{2-}$ at room temperature for Cu(II).

Table 1 reports the electrochemical properties of electrolytes tested with different concentrations of copper and hydrochloric acid obtained from cyclic voltammetries (CVs, Fig. 3) in a three-electrode conventional cell. The electrolytes have been evaluated in term of peak potentials of the anodic and cathodic processes (E_+ and E_-), separation between the peak potentials (ΔE), potential of the redox couple Cu(I)/Cu(II) calculated by the half-sum of the peak potentials, anodic and cathodic peak current densities (i_{pa} and i_{pc}) and their ratios. Varying the chloride concentration from 1 to 6 M, the current values increase as a consequence of the higher conductivity, and also the reversibility increase. Indeed, the i_{pa}/i_{pc} ratio gets close to 1, and the ΔE diminishes. On the other hand, the $(E_+ + E_-)/2$ of the process shifts towards positive potential. This effect does not depend on the enhanced conductivity but refers to the different equilibria involving the redox species, suggesting the chemical stabilization of the redox forms.

Moreover, decreasing the HCl from 6 to 1 M makes both anodic and cathodic peaks less evident. If the concentration of Cl^- is not high enough, Cu(I) is not stabilized and can disproportionate or be oxidized forming Cu(II) at the electrode interphase. Hence, the cathodic current is given by the combination of the electrochemical reduction of Cu(II) to Cu(I) and the chemical-electrochemical process involving the reduction of newly formed Cu(II). Indeed, the Cu(I) concentration at the electrode decreases, and there is less cuprous cation for oxidation at the electrode.

3.2. *Quantum chemical calculations: structures and electronic transitions of water solvated copper-chloride clusters*

Quantum chemical calculations were performed to interpret the variations observed in the experimental absorption spectra (see Fig. 1) of copper-chloride complexes by increasing the HCl concentration. Fig. 4a (top panel) shows the optimized lowest-energy supramolecular clusters (see section Calculations) for the water solvated species $[CuCl(H_2O)_5]^+$, $[CuCl_2(H_2O)_4]^0$, and $[CuCl_3(H_2O)_3]^-$. Clusters with a variable number of water molecules (up to 200) were also taken into account and results are reported in Supplementary Information. We observed that by increasing the number of ligands the Cu-Cl distance lowers from 2.24 Å for $[CuCl]^+$ to 2.15–2.08 Å for $[CuCl_3]^-$ showing, for the latter, strong metal-ligand interactions. Similarly, the distance between the copper ion and the oxygen atom of the nearest-neighbor solvated water molecules shrinks from 2.27/2.11 to 1.88 Å, showing relevant local non-bonded interactions. Furthermore, from a preliminary analysis of the radial distribution function between the copper ion and the oxygen atoms $g_{Cu\text{-}O}(r)$, calculated on supramolecular clusters featuring 50 to 200 water molecules (as optimized at the GFN2-xTB level, see Supplementary Information), we observed that by moving from $[CuCl]^+$ to $[CuCl_3]^-$ $g_{Cu\text{-}O}(r)$ decreases, as well as the total number of nearest-neighbor water molecules (i.e., first solvation shell) solvating the metal ion. Such result, though preliminary as being not based on extended and equilibrated molecular dynamics simulations (subject for next investigations), suggests that by increasing the number of chlorine ions, the amount of water molecules accessible to solvate the metal-ion center decreases. Our structural data are in good agreement with previously reported computational studies [36–38].

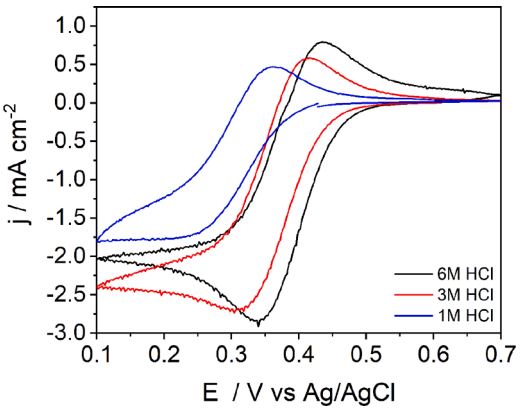

Fig. 3. CVs at 0.01 V s^{-1} and 40 °C of 50 mM $CuCl_2$ electrolytes with different concentrations of HCl in three-electrode conventional cell, WE: Pt disk, CE: graphite rod, RE: Ag/AgCl.

The ground-to-excited state electronic transitions of each cluster were computed both at the sTDA/sTD-DFT and TD-DFT levels. Here we discuss only TD-DFT results.

Fig. 4b (bottom left panel) shows the computed (vertical) excited state transitions for the three clusters $[CuCl(H_2O)_5]^+$, $[CuCl_2(H_2O)_4]^0$, and $[CuCl_3(H_2O)_3]^-$ in two spectral regions: 100–600 nm and 600–1050 nm. By increasing the number of chlorine ions (see $[CuCl_2(H_2O)_4]^0$ and $[CuCl_3(H_2O)_3]^-$), intense transitions appear in the 200–300 nm spectral region (TDDFT energies are unscaled). Such excitations can be assigned to single-particle transitions from *multiple* occupied molecular orbitals to the lowest unoccupied molecular orbital (LUMO). For both $[CuCl_2(H_2O)_4]^0$ and $[CuCl_3(H_2O)_3]^{-1}$ the occupied molecular orbitals involved in the transitions can be described as linear combinations of ligand-metal atomic orbitals of p- and d-type (see Supplementary Information for some examples), as delocalized over the cluster. Partial contributions are also borrowed from the molecular orbitals of the closest interacting water molecules. The LUMO is instead confined in the tetrahedral plane as defined by the copper-chlorine ions and it involves d-type atomic orbitals of the metal combined also with the unoccupied orbitals of the closest interacting water molecules (see Supplementary Information). Such transitions are of type LMCT and they can be assigned to the observed broad absorption band at around 250 nm, Fig. 1.

For both $[CuCl_2(H_2O)_4]^0$ and $[CuCl_3(H_2O)_3]^-$ weak bands are also present around 400 and 500 nm. Such transitions are weak LMCT excitations involving various occupied molecular orbitals and the LUMO. We assigned these bands to the absorption shoulder (at 400 nm) observed in the experimental spectra by increasing the HCl concentration (Fig. 1).

The cluster $[CuCl(H_2O)_5]^+$ shows intense high energy electronic transitions (below 200 nm, see Fig. 4b bottom left panel), however it does not show any prominent dipole allowed electronic transitions neither in the 250–300 nm region nor at lower energy (i.e., higher wavelength).

Notably, a distinguished transition is computed around 900 nm

Table 1
Electrochemical properties on Pt at 0.01 V s^{-1} and 40 °C of copper electrolytes with different concentrations of HCl in three-electrode conventional cell, WE: Pt disk, CE: graphite rod, RE: Ag/AgCl. The relative errors of potential measurements are ca. 0.5% and those related to the current measurements are ca. 2%.

$CuCl_2$ mM	HCl M	E_+ V vs. Ag/AgCl	E_- V vs. Ag/AgCl	ΔE V	$(E_+ + E_-)/2$ V vs. Ag/AgCl	i_{pa} mA cm^{-2}	$\lvert i_{pc}\rvert$ mA cm^{-2}	$i_{pa}/\lvert i_{pc}\rvert$
50	1	0.361	0.227	0.134	0.294	1.02	1.72	0.59
50	3	0.415	0.309	0.106	0.362	2.14	2.62	0.82
50	6	0.438	0.338	0.100	0.388	2.50	2.70	0.93

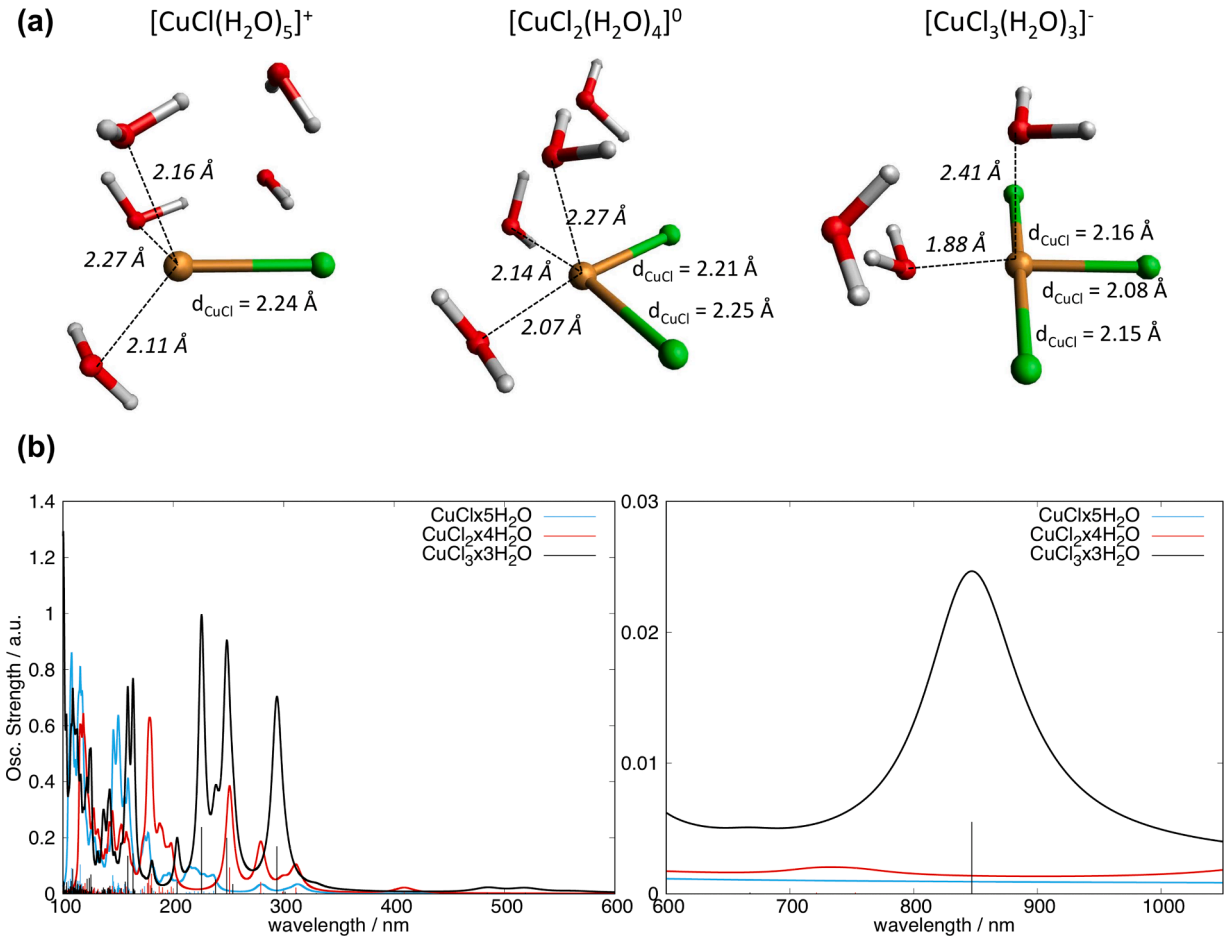

Fig. 4. Top panel, (a): optimized $[CuCl(H_2O)_5]^+$, $[CuCl_2(H_2O)_4]^0$, and $[CuCl_3(H_2O)_3]^-$ clusters, showing the relevant interatomic distances (Å). Bottom panels, (b): Computed TD-DFT electronic transitions (sticks) and absorption spectra (solid lines, Lorentzian convolution) for $[CuCl(H_2O)_5]^+$, $[CuCl_2(H_2O)_4]^0$, and $[CuCl_3(H_2O)_3]^-$ clusters (respectively, light-blue, red and black lines). Two spectral regions are reported: 100–600 nm and 600–1050 nm. TD-DFT energies are not scaled.

(Fig. 4b bottom right panel) for the $[CuCl_3(H_2O)_3]^-$ cluster. Such excitation is characterized by a very low oscillator strength ($f = 5 \times 10^{-3}$) as compared to those of the 200–300 nm region ($f = 2 \times 10^{-1}$), and it can be described as a pure HOMO-LUMO transition, showing a clear LMCT character. The cluster, $[CuCl(H_2O)_5]^+$ does not show such excitation, whereas the $[CuCl_2(H_2O)_4]^0$ shows it though featuring a very low oscillator strength ($f < 10^{-3}$). Consequently, based on the model-clusters here considered, we can assign the NIR transitions around 900 nm (Fig. 6) to Cu(II) clusters coordinated with an increased number of chloride ions, in particular to $[CuCl_3]^-$ species.

3.3. Cu(II) speciation dependence from Cu(II) concentration

As indicated in Eq. (2), the copper speciation is more influenced by the chloride concentration instead of the copper concentration. In a 5 mM Cu(II) 6 M HCl solution, the deconvolution of the UV/Vis absorption spectrum (Fig. 5a) shows a copper speciation comparable to that observed in 50 mM $CuCl_2$ 6 M HCl (speciation of copper in Fig. 1).

Based on our deconvolution (Fig. 1) and quantum-chemical (Fig. 4) analyzes, the absorption spectrum of Cu(II) chloride-rich solution can be described by an intense LMCT band in the UV region, and one in the NIR region. The latter correspond to a broad band that is weakly influenced by the Cu(II) coordination. Furthermore, this transition is characteristic of the Cu(II) and is not visible in Cu(I) solution.

In order to monitor the Cu(II) concentration by the NIR transition, a wavelength of 870 nm (λ_{abs}) was selected as probe. Indeed, the NIR transition results useful for the Cu(II) monitoring because of the low molar extinction coefficient (60–90 M^{-1} cm^{-1}) that allow the absorbance measurements even in highly concentrated solutions like those of practical interest in CuRFB. Voltabsorbometric experiments (Fig. 5b and c) were carried out by recording CVs and absorption spectra simultaneously. The CV of the 5 mM $CuCl_2$ solution reported in Fig. 5b shows Nernstian reversibility, as evinced by the separation between the cathodic and the anodic peak potentials (ΔE<2.22 RT/F that corresponds to 59 mV at 40 °C) [39]. The current ratio $i_{pa}/i_{pc} = 0.96$ indicates a decent stability of the Cu(I) in the chloride environment.

The absorbance percentage in Fig. 5b follow the variation of Cu(II) concentration. During the reduction process in the voltametric experiment, the concentration of Cu(II) decrease in favor of the Cu(I). Consequently, the absorbance percentage of the electrolyte decreases approaching zero. Then, the absorbing species are regenerated upon re-oxidation of Cu(I) to Cu(II), and the absorbance percentage returns at the initial value. The absorbance variation during CV is characterized by a hysteresis that can be related to the presence of metastable species. In particular, the signal recorded during the reduction scan is originated by the electrochemical reaction of cupric stable species producing metastable ones. Then, the backward reaction involves the reactivity of a cuprous metastable species with facilitated oxidation. Thus, the absorbance profile of the backward scan of the cyclic voltammetry anticipates the forward reduction due to the metastability of the reduced species (Cu(I)). The absorbance variation and hysteresis are related to all the copper chlorocomplexes present in the solution.

The absorbance percentage at 385 nm, where only the most stabilized complexes absorb ($[CuCl_3]^-$ and $[CuCl_4]^{2-}$), displays a decreased

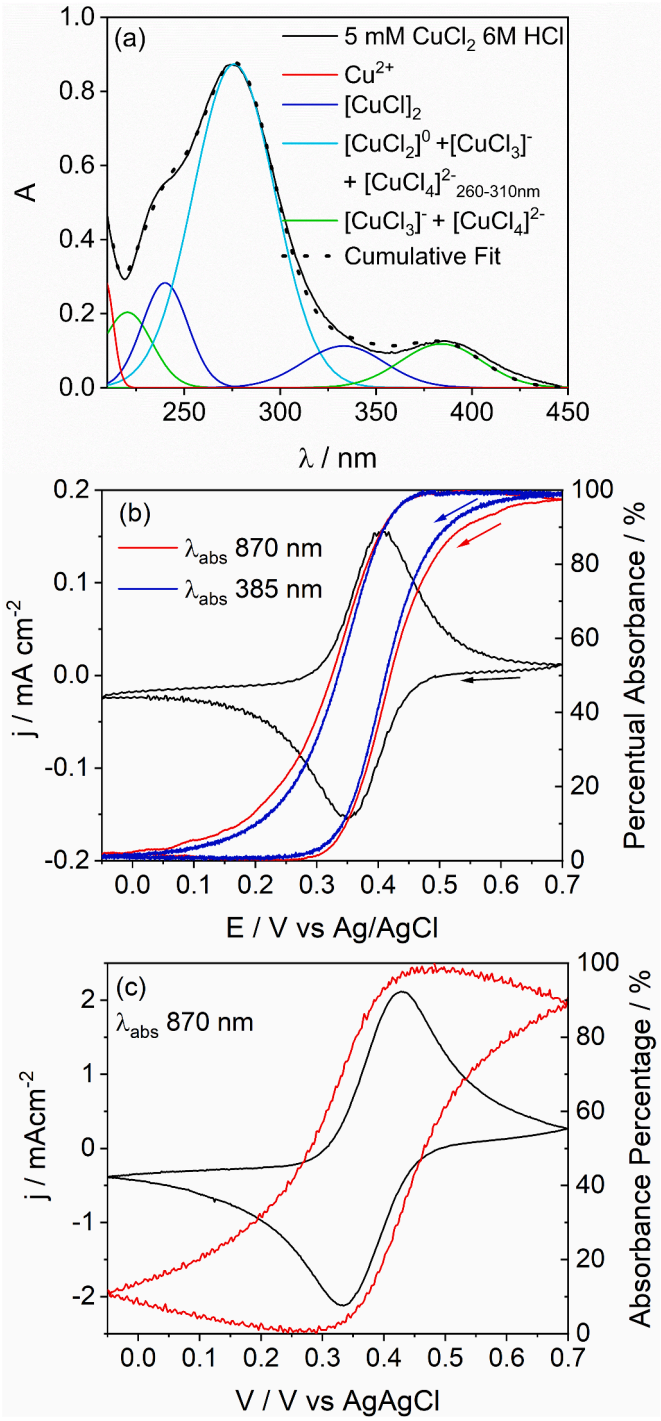

Fig. 5. (a) UV/Vis spectra of 5 mM $CuCl_2$ 6 M HCl electrolyte in quartz cuvette (OP 50 μm), (b) CV at 2 mV s^{-1} in 5 mM $CuCl_2$ 6 M HCl monitoring the absorbance at 385 nm and 870 nm (OP 10 mm), WE: Pt mesh, CE: Pt wire, RE: Ag/AgCl. (c) CV at 2 mV s^{-1} in 50 mM $CuCl_2$ 6 M HCl monitoring the absorbance at 870 nm (OP 10 mm), WE: Pt mesh, CE: Pt wire, RE: Ag/AgCl.

hysteresis suggesting less interaction factors. Thus, a prevalence of high coordinated copper cation is suggested. The deconvolution of the LMCT band when the copper concentration is increased by ten times, from 5 to 50 mM, indicates an increased concentration of $[CuCl_x]^{2-x}$ with $x<3$. Analogously, the absorbance profile at 870 nm exhibits a stronger hysteresis imputable at the increased concentration of metastable species.

Fig. 5c reports the CV of a 50 mM $CuCl_2$ solution in 6 M HCl and the absorbance values were recorded at 870 nm during the CV. The wavelength was selected close to the maximum of the absorption spectrum of the solution. Even if the CV is characterized by a i_{pa}/i_{pc} ratio closer to 1, the reported abrsorbance curve suffers an higher hysteresis due to the less stabilized complexes $[CuCl_2]^0$, $[CuCl]^+$ and Cu^{2+}. Indeed, the signal increases in the forward scan of the voltammetry after the minimum (mostly Cu(I) in solution) and decrease in the backward scan after reaching the maximum (mostly Cu(II)).

Hence, NIR spectroscopy results a suitable and sensible techniques to compare different complexes distributions. The hysteresis evidenced in the absorbance profile can be ascribed to the higher presence of less stabilized complexes (Cu^{2+}/$[CuCl]^+$/$[CuCl_2]^0$) with respect to 5 mM $CuCl_2$ 6 M HCl solution.

To achieve the condition required for a highly performing redox flow battery, is mandatory to increase the copper concentration. It is important to consider that at high concentrations also other factors contributes to the electrochemical properties of the electrolyte.

Specifically, the salt solubility and diffusion coefficients are of paramount importance in these systems. The diffusion coefficients (D) of both Cu^+ and Cu^{2+} range from 10^{-5} to 10^{-6} cm^2 s^{-1}, with $D(Cu^+)$ higher than $D(Cu^{2+})$, the higher is the temperature the higher are the D values [40]. However, the increase of the copper concentration, needed to RFB for delivering high energy, brings a tremendous increase of the ionic strength of the solution to maintain a suitable copper-to-halide ratio. In these conditions, the interactions between ions are stronger, and the decrease of water activity highly affects the physicochemical parameters like viscosity and density, as well as the conductivity and the diffusion coefficient [41,42].

The Cu(II) concentration was increased from 5 to 2 M in 6 M HCl solutions. In this range of concentrations, the absorbance has been monitored in the NIR region taking advantage of the low molar extinction coefficient. The wide range of concentrations required the use of cuvettes with different OP for not having deviation from linearity of the absorbance with the increasing of Cu(II) concentration.

The absorbance of 5 mM Cu(II) solution shows a maximum at 930 nm while the solutions with higher concentrations have the maximum at 920 nm. The small bathochromic shift suggests a decrease in the Cu(II) coordination as also confirmed by the chlorocomplex distribution at different Cu(II) concentrations (Fig. 2). Despite the difference in magnitude, there is little variation in the distribution of complexes between the 5 and 50 mM. Similarly, the concentration increase by a further order of magnitude would not be expected to produce a much larger variation in the Cu(II) coordination. In fact, no differences are evidenced in the shape of the NIR absorption spectra (Fig. 6a–d).

Table 2 summarizes the electrochemical information obtained by CVs in a spectroelectrochemical cell (showed in Figs. 5a-5b). The spectroelectrochemical cell geometry limits the electrochemical investigation to 0.05 M copper solution due to the absence of compartment separation. The high currents reached in highly concentrated electrolytes lead to massive gas evolution at the CE (in the foreword scan), inducing convective motions that affect mass transport. For this reason, the 0.5 M and 2 M $CuCl_2$ 6 M HCl electrolyte has been evaluated in three-electrode conventional cell on a Pt disk working electrode (Fig. S2). This could be related to the lower coordination of the copper as well as to other limitations due to the higher concentration (e.g., high ionic strength, high viscosity, lower diffusion coefficient etc.). As expected, the current densities increase with the raising of the concentration of the redox active species. However, it should be noted that the comparison of the currents is problematic because of the two different cell configurations used. The analysis of the i_{pa}/i_{pc} ratio demonstrates that the system behaves as quasi reversible for all the investigated concentrations, with a mean value of 0.99 ± 0.03 (and the error in the i_{pa}/i_{pc} values around 0.04).

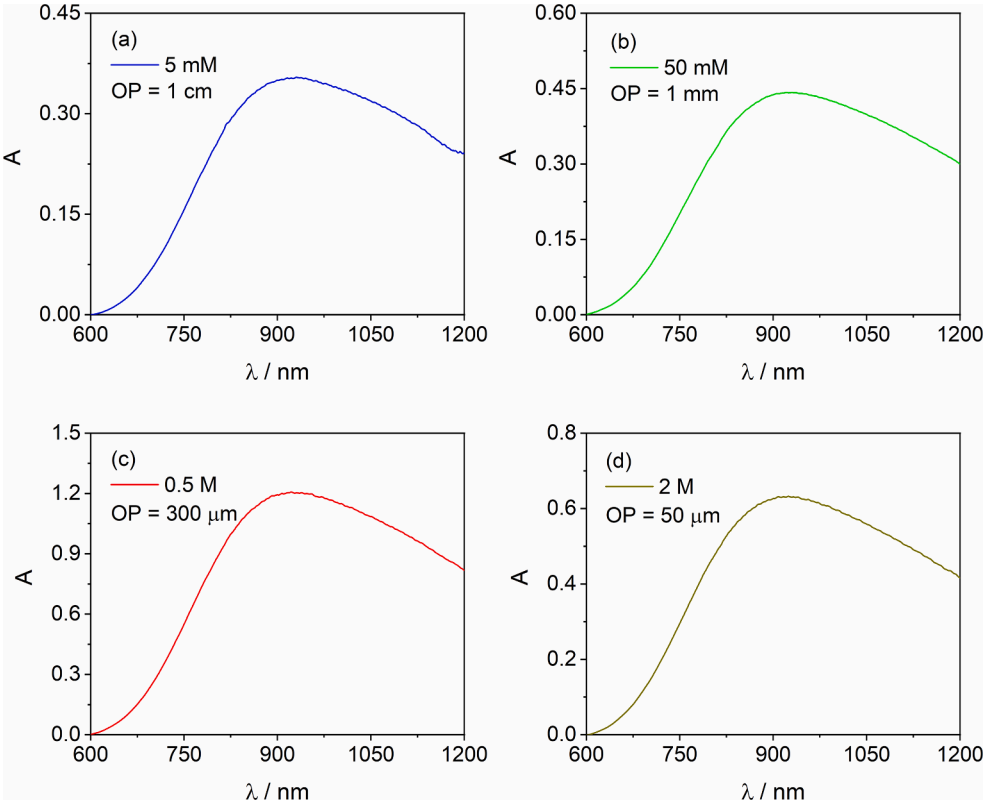

Fig. 6. NIR spectra of (a) 5 mM $CuCl_2$ 6 M HCl electrolyte (OP 10 mm), (b) 50 mM $CuCl_2$ 6 M HCl electrolyte (OP 1 mm), (c) 0.5 M $CuCl_2$ 6 M HCl electrolyte (OP 300 μm), and (d) 2 M $CuCl_2$ 6 M HCl electrolyte (OP 50 μm) in quartz cuvette.

Table 2
Electrochemical properties on Pt at 0.01 V s^{-1} of copper electrolytes. 0.005 and 0.05 M $CuCl_2$ electrolytes have been evaluated in the spectroelectrochemical cell (SPE), WE: Pt mesh, CE: Pt wire, RE: Ag/AgCl. 0.5 and 2 M $CuCl_2$ electrolytes have been evaluated in a three-electrode conventional cell (CON), WE: Pt disk (4 mm), CE: graphite rod, RE: Ag/AgCl. The relative errors of potential measurements are ca. 0.5% and those related to the current measurements are ca. 2%.

$CuCl_2$ M	HCl M	E_+ V vs. Ag/AgCl	E_- V vs. Ag/AgCl	ΔE V	$(E_+ + E_-)/2$ V vs. Ag/AgCl	i_{pa} mA cm^{-2}	$\lvert i_{pc}\rvert$ mA cm^{-2}	$i_{pa}/\lvert i_{pc}\rvert$	Cell
0.005	6	0.404	0.355	0.049	0.380	0.14	0.15	0.96	SPE
0.05	6	0.427	0.334	0.093	0.380	2.12	2.05	1.03	SPE
0.5	6	0.420	0.340	0.080	0.380	28.0	29.1	0.96	CON
2	6	0.419	0.305	0.114	0.362	109	109	1.00	CON

4. Conclusions

The optimization of new electrolytes plays a crucial role in developing a highly-performing CuRFB. In this system, the presence of chlorides as ligands is essential to stabilize the Cu(I)-to-Cu(II) process occurring in the positive compartment of the redox flow cell.

UV–Vis spectroscopy, supported by quantum-chemical modeling, allowed the investigation of the copper complexes distributions in diluted solutions from the analysis of the LMCT bands. Tight-binding-DFT and DFT calculations revealed the structure of water solvated copper-chloride clusters, showing that by increasing the number of chlorine ions ($[CuCl(H_2O)_5]^+$, $[CuCl_2(H_2O)_4]^0$, and $[CuCl_3(H_2O)_3]^-$), the amount of water molecules accessible to solvate the metal-ion center decreases. Through TDDFT calculations the electronic transitions of the supramolecular clusters were characterized, identifying the LMCT excitations both in the UV–Vis and NIR regions. By increasing the number of chlorides, NIR LMCT transitions activate for Cu(II). The absorbance of Cu(II) at different wavelengths during CVs showed an hysteresis due to the different distribution of chlorocomplexes The absorbance hysteresis in the NIR, namely at 870 nm where all the Cu(II) complexes absorb, is more evident than at 385 nm, where the absorptions of the most stabilized complexes ($[CuCl_3]^-$ and $[CuCl_4]^{2-}$) also overlap. Thus, highly coordinated copper cations are recommended to increase the reversibility of the Cu(I)/Cu(II) redox process.. Small shift in the NIR band and no shape variation suggest no significant differences in the Cu(II) speciation, among low and high concentrated solutions, also confirmed by comparing the electrochemical properties of 0.05 and 0.5 M $CuCl_2$ solutions. NIR bands allow the study of highly concentrated systems by tuning the optical path of the cell and can be used to monitor the Cu(II) concentration and the state of charge in the CuRFB.

CRediT authorship contribution statement

Giampaolo Lacarbonara: Conceptualization, Investigation, Data curation, Visualization, Writing – original draft, Writing – review & editing. **Nicolò Albanelli:** Conceptualization, Investigation, Data

curation, Writing – review & editing. **Daniele Fazzi:** Methodology, Validation, Formal analysis, Writing – review & editing. **Catia Arbizzani:** Supervision, Resources, Conceptualization, Supervision, Project administration, Funding acquisition, Writing – review & editing.

Declaration of Competing Interest

The authors declare that they have no known competing financial interests or personal relationships that could have appeared to influence the work reported in this paper.

Acknowledgments

This work was supported by the European Union within the Horizon 2020 research and innovation program [CUBER - Copper-Based Flow Battery for Energy storage Renewables Integration H2020 - LC - BAT_2019] under grant agreement No. 875605. All the Project Partners are acknowledged for the fruitful discussion. G.L. acknowledges the Department of Excellence program financed by the Minister of Education, University and Research (MIUR, L. 232 del December 01/12/2016) for the doctoral scholarship. D. F. acknowledges partial funding from the National Recovery and Resilience Plan (NRRP), Mission 04 Component 2, Investment 1.5 – NextGenerationEU, Call for tender n. 3277 dated 30/12/2021, Award Number: 0001052 dated 23/06/2022.

Supplementary materials

Supplementary material associated with this article can be found, in the online version, at doi:10.1016/j.electacta.2023.142514.

References

[1] D. Gielen, F. Boshell, D. Saygin, M.D. Bazilian, N. Wagner, R. Gorini, The role of renewable energy in the global energy transformation, Energy Strat. Rev. 24 (2019) 38–50, https://doi.org/10.1016/j.esr.2019.01.006.
[2] M. Skyllas-Kazacos, M.H. Chakrabarti, S.A. Hajimolana, F.S. Mjalli, M. Saleem, Progress in flow battery research and development, J. Power Sources 160 (2006) 716–732, https://doi.org/10.1149/1.3599565.
[3] B. Kratochvil, K.R. Betty, A secondary battery based on the copper(II)-(I) and (I)-(0) couples in acetonitrile, J. Electrochem. Soc. 121 (1974) 851–854, https://doi.org/10.1149/1.2401935.
[4] W.W. Porterfield, J.T. Yoke, Room Temperature Fused Salts: Liquid Chlorocuprates (I), in: R. Bruce King (Ed.), Advances in Chemistry - Inorganic Compounds with Unusual Properties Vol. 150, ACS Publications, Washington, DC, 1976, pp. 104–111, https://doi.org/10.1021/ba-1976-0150.ch010. Ch. 10.
[5] L. Sanz, J. Palma, E. García-Quismondo, M. Anderson, The effect of chloride ion complexation on reversibility and redox potential of the Cu(II)/Cu(I) couple for use in redox flow batteries, J. Power Sources 224 (2013) 278–284, https://doi.org/10.1016/j.jpowsour.2012.10.005.
[6] J. Blumberger, L. Bernasconi, I. Tavernelli, R. Vuilleumier, M. Sprik, Electronic structure and solvation of copper and silver ions: a theoretical picture of a model aqueous redox reaction, J. Am. Chem. Soc. 126 (12) (2004) 3928–3938, https://doi.org/10.1021/ja0390754.
[7] D. Lloyd, T. Vainikka, K. Kontturi, The development of an all-copper hybrid redox flow battery using deep eutectic solvents, Electrochim. Acta 100 (2013) 18–23, https://doi.org/10.1016/j.electacta.2013.03.130.
[8] E.A. Stricker, K.W. Krueger, R.F. Savinell, J.S. Wainright, Investigating a bromide supported electrolyte for an all-copper flow battery, J. Electrochem. Soc. 165 (2018) 9, https://doi.org/10.1149/2.1031809jes. A1797-A1804.
[9] L. Sanz, W.D. Badenhorst, G. Lacarbonara, L. Faggiano, D. Lloyd, P. Kauranen, C. Arbizzani, L. Murtomäki, All-copper flow batteries, in: C. Roth, J. Noack, M. Skyllas-Kazacos, Part 5: Chemistries Other Than Vanadium, Flow Batteries From Fundamentals to Applications, Vol. 2, Ch. 38 (2023) 855–873, DOI:10.1002/9783527832767.
[10] W.D. Badenhorst, L.S. Kuldeep, C. Arbizzani, L. Murtomäki, Performance improvements for the all-copper redox flow battery: membranes, electrodes, and electrolytes, Energy Rep. 8 (2022) 8690–8700, https://doi.org/10.1016/j.egyr.2022.06.075.
[11] S. Ahrland, J. Rawsthorne, The stability of metal halide complexes in aqueous solution. VII The chloride complexes of copper (I), J. Acta Chem. Scand. 24 (1970) 157–172, https://doi.org/10.3891/acta.chem.scand.24-0157.
[12] J.J. Fritz, Chloride complexes of copper(I) chloride in aqueous solution, J. Phys. Chem. 84 (1980) 2241–2246, https://doi.org/10.1021/j100455a006.
[13] J.J. Fritz, Solubility of cuprous chloride in various soluble aqueous chlorides, J. Chem. Eng. Data 27 (1982) 188–193, https://doi.org/10.1021/je00028a027.
[14] W. Liu, D.C. McPhail, Thermodynamic properties of copper chloride complexes and copper transport in magmatic-hydrothermal solutions, Chem. Chem. Geol. 221 (2005) 21–39, https://doi.org/10.1016/j.chemgeo.2005.04.009.
[15] M. Lundström, J. Aromaa, O. Forsén, Redox potential characteristics of cupric chloride solutions, Hydrometallurgy 95 (2009) 285–289, https://doi.org/10.1016/j.hydromet.2008.06.009.
[16] M. Lundström, J. Aromaa, O. Forsén, O. Hyvärinen, M.H. Barker, Cathodic reactions of Cu^{2+} in cupric chloride solution, Hydrometallurgy 85 (1) (2007) 9–16, https://doi.org/10.1016/j.hydromet.2006.07.002.
[17] R.W. Ramette, G. Fan, Copper(II) chloride complex equilibrium constants, Inorg. Chem. 22 (1983) 3323–3326, https://doi.org/10.1021/ic00164a029.
[18] R.W. Ramette, Copper(II) complexes with chloride ion, Inorg. Chem. 25 (1986) 2481–2482, https://doi.org/10.1021/ic00234a044.
[19] A. Nelson, R.F.C. Mantoura, Voltammetry of copper species in estuarine waters: part I. Electrochemistry of copper species in chloride media, J. Electroanal. Chem. Interfacial Electrochem. 164 (2) (1984) 237–252, https://doi.org/10.1016/S0022-0728(84)80209-0.
[20] T. Vainikka, D. Lloyd, L. Murtomäki, J.A. Manzanares, K. Kontturi, Electrochemical study of copper chloride complexes in the RTIL 1-butyl-1-methylpyrrolidinium bis(trifluoromethylsulfonyl)imide, Electrochim. Acta 87 (2013) 739–748, https://doi.org/10.1016/j.electacta.2012.09.062.
[21] J. Vazquez-Arenas, I. Lazaro, R. Cruz, Electrochemical study of binary and ternary copper complexes in ammonia-chloride medium, Electrochim. Acta 52 (20) (2007) 6106–6117, https://doi.org/10.1016/j.electacta.2007.03.062.
[22] H. Zhao, J. Chang, A. Boika, A.J. Bard, Electrochemistry of high concentration copper chloride complexes, Anal. Chem. 85 (2013) 7696–7703, https://doi.org/10.1021/ac4016769.
[23] Y. Meng, A.J. Bard, Measurement of temperature-dependent stability constants of Cu(I) and Cu(II) chloride complexes by voltammetry at a Pt ultramicroelectrode, Anal. Chem. 87 (2015) 3498–3504, https://doi.org/10.1021/acs.analchem.5b00052.
[24] A.H. Whitehead, T.J. Rabbow, M. Trampert, P. Pokorny, Critical safety features of the vanadium redox flow battery, J. Power Sources 351 (2017) 1–7, https://doi.org/10.1016/j.jpowsour.2017.03.075.
[25] G. Lacarbonara, R. Petruzzelli, C. Arbizzani, State of charge monitoring in all-copper redox flow batteries, Manuscript in preparation.
[26] L. Martinez, R. Andrade, E.G. Birgin, J.M. Martinez, PACKMOL: a package for building initial configurations for molecular dynamics simulations, J. Comput. Chem. 30 (2009) 2157–2164, https://doi.org/10.1002/jcc.21224.
[27] C. Bannwarth, E. Caldeweyher, S. Ehlert, A. Hansen, P. Pracht, J. Seibert, S. Spicher, S. Grimme, Extended tight-binding quantum chemistry methods, WIREs Comput. Mol. Sci. 11 (2021) e1493, https://doi.org/10.1002/wcms.1493.
[28] S. Grimme, C. Bannwarth, P. Shushkov, A robust and accurate tight-binding quantum chemical method for structures, vibrational frequencies, and noncovalent interactions of large molecular systems parametrized for all spd-block elements (Z = 1–86), J. Chem. Theory Comput. 13 (2017) 1989–2009, https://doi.org/10.1021/acs.jctc.7b00118.
[29] C. Bannwarth, S. Ehlert, S. Grimme, GFN2-xTB—an accurate and broadly parametrized self-consistent tight-binding quantum chemical method with multipole electrostatics and density-dependent dispersion contributionsm, J. Chem. Theory Comput., 15 (2019) 1652–1671, https://doi.org/10.1021/acs.jctc.8b01176.
[30] P. Pracht, F. Bohle, S. Grimme, Automated exploration of the low-energy chemical space with fast quantum chemical methods, Phys. Chem. Chem. Phys. 22 (2020) 7169–7192, https://doi.org/10.1039/C9CP06869D.
[31] D. Figgen, G. Rauhut, M. Dolg, H. Stoll, Energy-consistent pseudopotentials for group 11 and 12 atoms: adjustment to multi-configuration Dirac–Hartree–Fock data, Chem. Phys. 311 (2005) 227, https://doi.org/10.1016/j.chemphys.2004.10.005.
[32] K.A. Peterson, C. Puzzarini, Systematically convergent basis sets for transition metals. II. Pseudopotential-based correlation consistent basis sets for the group 11 (Cu, Ag, Au) and 12 (Zn, Cd, Hg) elements, Theor. Chem. Acc. 114 (2005) 283, https://doi.org/10.1007/s00214-005-0681-9.
[33] S. Grimme, A simplified Tamm-Dancoff density functional approach for the electronic excitation spectra of very large molecules, J. Chem. Phys. 138 (2013), 244104, https://doi.org/10.1063/1.4811331.
[34] M.J. Frisch, et al., Gaussian 16, Revision C.01, Gaussian, Inc., Wallingford, 2016.
[35] J. Brugger, D.C. McPhail, J. Black, L. Spiccia, Complexation of metal ions in brines: application of electronic spectroscopy in the study of the Cu(II)-LiCl-H2O system between 25 and 90 C, Geoch. Cosmoch. Acta 65 (2001) 2691–2708, https://doi.org/10.1016/S0016-7037(01)00614-7.
[36] F.F. Xia, H.B. Yi, D. Zeng, Hydrates of copper dichloride in aqueous solution: a density functional theory and polarized continuum model investigation, J. Phys. Chem. A 113 (2009) 14029–14038, https://doi.org/10.1021/jp909092p.
[37] H.B. Yi, F.F. Xia, Q. Zhou, D. Zeng, $[CuCl_3]^-$ and $[CuCl_4]^{2-}$ hydrates in concentrated aqueous solution: a density functional theory and *ab initio* study, J. Phys. Chem. A 115 (2011) 4416–4426, https://doi.org/10.1021/jp109723v.
[38] F.F. Xia, H.B. Yi, D. Zeng, Hydrates of Cu^{2+} and $CuCl^+$ in dilute aqueous solution: a density functional theory and polarized continuum model investigation, J. Phys. Chem. A 114 (2010) 8406–8416, https://doi.org/10.1021/jp1000804.
[39] A.J. Bard, L. Faulkner. Electrochemical Methods: Fundamentals and Applications, John Wiley & Sons, Inc., New York, 2001.
[40] A.C.F. Ribeiro, M.A. Esteso, V.M.M. Lobo, A.J.M. Valente, S.M.N. Simoes, A.J.F. N. Sobral, H.D. Burrows, Diffusion coefficients of copper chloride in aqueous

solutions at 298.15K and 310.15K, J. Chem. Eng. Data 50 (2005) 1986–1990, https://doi.org/10.1021/je050220y.
[41] G. Lacarbonara, L. Faggiano, S. Porcu, P.C. Ricci, S. Rapino, D.P. Casey, J.F. Rohan, C. Arbizzani, Copper chloro-complexes concentrated solutions: an electrochemical study, Batteries 7 (2021) 83, https://doi.org/10.3390/batteries7040083.
[42] L. Faggiano, G. Lacarbonara, W.D. Badenhorst, L. Murtomäki, L. Sanz, C. Arbizzani, Short thermal treatments of carbon felts for copper-based redox flow batteries, J. Power Sources 520 (2022), 230846, https://doi.org/10.1016/j.jpowsour.2021.230846.